*American Mineralogist, Volume 72, pages 148–156, 1987*

# Chemistry and structure of esseneite ($CaFe^{3+}AlSiO_6$), a new pyroxene produced by pyrometamorphism*

MICHAEL A. COSCA, DONALD R. PEACOR
Department of Geological Sciences, University of Michigan, Ann Arbor, Michigan 48109, U.S.A.

## ABSTRACT

Esseneite, a new clinopyroxene with ideal formula $CaFe^{3+}AlSiO_6$ occurs with melilite, anorthite, solid solutions of magnetite-hercynite, and glass in paralava (fused sedimentary rock) associated with naturally combusted coal seams near Gillette, Wyoming. It is named for Eric Essene, Professor of Geology at the University of Michigan. Esseneite has space group $C2/c$ with $a = 9.79(1)$, $b = 8.822(9)$, $c = 5.37(1)$ Å and $\beta = 105.81(9)°$. Structure-refinement results are presented from an esseneite crystal from paralava with average pyroxene composition

$$(Ca_{1.01}Na_{0.01})\ (Fe^{3+}_{0.72}Mg_{0.16}Al_{0.04}Ti_{0.03}Fe^{2+}_{0.02}Mn_{0.00})\ (Si_{1.19}Al_{0.81})O_6.$$

The crystal structure has been refined to residuals of 0.046 (weighted) and 0.055 (unweighted) using 509 reflections. Sites are occupied by Ca and Na in M2, $Fe^{3+}$ and Mg in M1, and Al and Si in the tetrahedral site. There is no detectable $Fe^{3+}$ in the tetrahedral site in contrast to experimentally synthesized $CaFe^{3+}AlSiO_6$, which contains tetrahedral $Fe^{3+}$, implying a cooling rate dependence of $Fe^{3+}$ and Al ordering on the M1 and T sites, respectively.

From available experimental and thermodynamic data, the thermodynamic properties of esseneite have been calculated: $\Delta G^\circ_{298} = -2705.8$ kJ; $\Delta H^\circ_{298} = -2871.1$ kJ; and $S^\circ_{298} = 177.0\ J \cdot mol^{-1} \cdot K^{-1}$. Phase-equilibrium calculations suggest that esseneite is stabilized by reactions involving plagioclase, melilite, wollastonite, magnetite, and hercynite at high temperatures under conditions of high $f_{O_2}$ approaching the hematite-magnetite buffer.

## INTRODUCTION

Pyrometamorphic processes associated with the natural combustion of coal in the Powder River Basin, Wyoming, have produced slaglike masses of paralava derived from sedimentary protoliths (Cosca and Essene, 1985; Cosca et al., 1986 and ms. in prep.). Mineral assemblages within the slag (paralava) are locally silica undersaturated, and many contain clinopyroxenes enriched in the $CaFeAlSiO_6$ (Ca-$Fe^{3+}$-Al Tschermaks molecule) component, FATs. We describe here one such pyroxene separated from a paralava sample (DR-8) from near Gillette, Wyoming, containing pyroxenes with the average composition $(Ca_{1.01}Na_{0.01})(Fe^{3+}_{0.72}Mg_{0.16}Al_{0.04}Ti_{0.03}Fe^{2+}_{0.02}Mn_{0.00})(Si_{1.19}Al_{0.81})O_6$ (Table 1). The high proportion of Al in the tetrahedral site and $Fe^{3+}$ in the M1 octahedral site indicate that this is a new mineral species. Although end-member $CaFeAlSiO_6$ has been previously synthesized (e.g., Hijikata, 1968), this is the first known natural occurrence of a similar pyroxene.

Unfortunately, systematic definitions have not been applied to Ca-rich clinopyroxenes. It is here proposed that the dominant M1 cation be used to distinguish the name in Ca-rich pyroxenes [e.g., Mg: diopside; $Fe^{2+}$: hedenbergite; Mn: johannsenite; Zn: petedunnite (Essene and Peacor, 1987); $Fe^{3+}$: esseneite; $Sc^{3+}$: unnamed (Davis, 1984)]. Eventually pyroxenes may be found with Al, $Ti^{4+}$, or $Ti^{3+}$ dominant in the M1 site, which would also qualify as new pyroxene species. In this classification, fassaite in the sense defined by Deer et al. (1978) would be relegated to a variety of aluminous and ferrian diopside. In addition, salite would represent a ferroan diopside and ferrosalite a magnesian hedenbergite. Although many potential M1 substitutions exist in Ca-rich pyroxenes among the major divalent (Mg, Mn, Zn, $Fe^{2+}$), trivalent (Al, Fe, Sc, V, $Ti^{3+}$) and tetravalent ($Ti^{4+}$) cations, there is a restricted range of substitutions in nature. For example, pyroxenes with large amounts of the CaTs (Ca-Tschermaks molecule) component have been described from eclogite inclusions in kimberlites (Dobretsov, 1968; Deer et al., 1978; Shatskiy et al., 1985), granulites (Kornprobst et al., 1982; Lal et al., 1984), alkaline igneous rocks including carbonatites (Peacor, 1967; LeBas, 1962; Treiman, 1982), contact metamorphic rocks (Deer et al., 1978; Hall, 1980; Devine and Sigurdsson, 1980; Williams-Jones, 1981), and in meteorites (Dodd, 1971; Hazen and Finger, 1977; Prinz et al., 1977). Fassaites rich in $Ti^{3+}$ and/or $Ti^{4+}$ have been described from meteorites as well (Dowty

* Contribution no. 418 from the Mineralogical Laboratory, Department of Geological Sciences, University of Michigan.

0003–004X/87/0102–0148$02.00

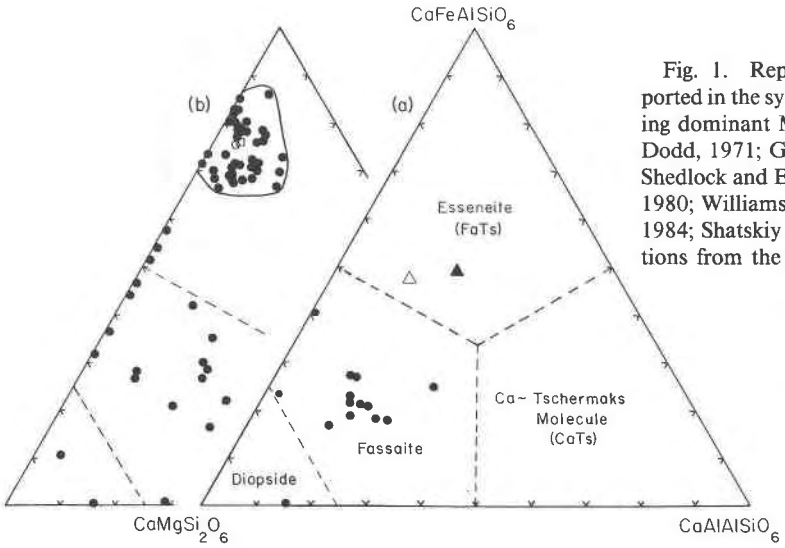


Fig. 1. Representative natural pyroxene compositions reported in the system $CaMgSi_2O_6$-$CaFeAlSiO_6$-$CaAlAlSiO_6$ showing dominant M1 site occupancy. (a) Data from Peacor, 1967; Dodd, 1971; Gross, 1977; Prinz et al., 1977; Deer et al., 1978; Shedlock and Essene, 1979; Devine and Sigurdsson, 1980; Hall, 1980; Williams-Jones, 1981; Kornprobst et al., 1982; Lal et al., 1984; Shatskiy et al., 1985. Also shown are pyroxene compositions from the Mottled Zone (△), from a calc-silicate xenolith from a kimberlite (▲), and (b) from paralava (this work). For sample DR-8, the enclosed area represents the compositional range of 43 separated pyroxene grains; □ = the average chemical analysis. Also shown is a pyroxene composition (○) from paralava collected independently by Foit and Hooper (pers. comm.).

and Clark, 1973). In contrast to the more common CaTs substitution (AlAl = MgSi), the FATs substitution ($Fe^{3+}$·Al = MgSi) is unusual but has been reported as a major component of pyroxenes within eclogite inclusions from kimberlites (Shatskiy et al., 1985) and from pyrometamorphic rocks from the Mottled Zone, Israel (Gross, 1977). The range of reported pyroxene compositions within the system $CaMgSi_2O_6$-$CaAlAlSiO_6$-$CaFeAlSiO_6$ is illustrated in Figure 1 with pyroxene compositions from paralava shown for comparison. The dashed lines separate fields for which the cations Mg, $Fe^{3+}$, and Al are dominant in the M1 sites, representing different pyroxene species. In addition a line has been drawn to separate diopside from the fassaite field with $0.25 < {}^{IV}Al < 0.50$. As shown, two previously reported pyroxenes, one from the Mottled Zone (Gross, 1977) and one from a calc-silicate xenolith from a kimberlite pipe (Shatskiy et al., 1985) would also qualify as esseneite.

We take great pleasure in naming this mineral esseneite in honor of Dr. Eric J. Essene, Professor at the University of Michigan, who first brought it to our attention, in recognition of his many contributions to mineralogy and the understanding of mineral equilibria. The new mineral and the name were approved, prior to publication, by the Commission on New Minerals and Mineral Names, IMA. Type material is preserved at the Smithsonian Institution (NMNH no. 163357).

## Occurrence

Esseneite occurs with anorthite, melilite solid solutions, magnetite-hercynite solid solutions, and glass within a slaglike crystalline matrix of paralava (Cosca and Essene, 1985). Paralava is defined as a fusion product of sediments overlying and associated with naturally combusted coal seams, and although it is mostly crystalline, a glass phase is usually present in small amounts. Minerals found in other Wyoming paralavas include fayalitic olivine ($Fo_{<10}$), tridymite, melilite solid solutions ($Na\text{-}mel_{1-28}Ak_{57-82}Geh_{15-28}$), spinel solid solutions ($Mt_{30-80}$-$Hc_{13-60}Uv_{2-13}$), nepheline, cordierite, wollastonite, hematite, and apatite. The pyroxene described in this paper comes from a paralava outcrop located on the Durham Ranch, about 13 km northeast of Reno Junction and 25 km south of Gillette, Wyoming. Paralava and associated baked sediment (sometimes referred to as clinker) cover approximately 37 000 km² in eastern Wyoming in

Table 1. Chemical analyses of esseneite

| | Sample DR-8 | |
|---|---|---|
| | Avg.* | Crystal** |
| $SiO_2$ | 29.51 | 33.20 |
| $TiO_2$ | 0.99 | 0.78 |
| $Al_2O_3$ | 17.95 | 11.90 |
| $Fe_2O_3$† | 23.89 | 21.39 |
| FeO | 0.69 | 5.15 |
| MnO | 0.11 | 0.08 |
| MgO | 2.68 | 4.39 |
| CaO | 23.40 | 22.65 |
| $Na_2O$ | 0.14 | 0.34 |
| Sum | 99.36 | 99.88 |
| Si | 1.188 | 1.329 |
| $^{IV}Al$ | 0.812 | 0.562 |
| $^{IV}Fe^{3+}$ | 0 | 0.109 |
| $^{VI}Al$ | 0.039 | 0 |
| $Fe^{3+}$ | 0.724 | 0.542 |
| $Fe^{2+}$ | 0.023 | 0.173 |
| Ti | 0.030 | 0.023 |
| Mg | 0.161 | 0.262 |
| Mn | 0.004 | 0.003 |
| Ca | 1.009 | 0.972 |
| Na | 0.011 | 0.026 |

* Average of 43 individual analyses conducted on separate grains from a prepared grain mount.
** Analysis of a portion of the refined crystal.
† Calculated from normalized formula.

the form of erosionally resistant mesas and buttes (Cosca et al., ms. in prep.). These Wyoming clinker outcrops represent one portion of a semicontinuous belt of clinker beds covering 500 000 km² stretching from Texas to British Columbia (Bentor, 1984). Similar, although less extensive occurrences of clinker formed by natural coal combustion have been described from Australia, Canada, India, New Zealand, and Russia (Bentor et al., 1981).

Minimum formation temperatures of Wyoming paralava are found to be in the range 1200–1600°C (Cosca and Essene, 1985) based on microprobe analyses of the glass phase compared to 1-atm liquidus phase diagrams. The particular mineral assemblage produced in paralava is partly a function of the temperature, degree of partial melting, and oxidation state related to local gas buffers, in addition to the original bulk composition of the sedimentary protolith (Cosca and Essene, 1985). These variables are evidenced by the large variation in chemistry of pyroxenes from paralava (Fig. 1). The estimated high temperature and low pressure, combined with relatively rapid crystallization, have produced a myriad of lath-shaped anorthite and melilite solid solutions, euhedral magnetite-hercynite spinels, prismatic pyroxenes, and interstitial glass. Textures observed in thin sections are similar to those of fine-grained volcanic rocks.

Other types of combustion metamorphic (pyrometamorphic) rocks have been observed associated with bituminous mudstones (Bentor et al., 1981) and organic-rich carbonates (Gross, 1977). The compositions and mineralogy of the associated rocks from these different environments are highly variable, reflecting in large part differences in initial bulk chemistry of the protolith (Bentor, 1984).

## Physical and optical properties

Esseneite occurs as prismatic crystals 2–8 mm in length and is reddish-brown in color with the tone being darker with increasing total Fe content. The crystals exhibit perfect {110} cleavage and display a vitreous luster on both crystal faces and fracture surfaces. Esseneite is transparent in thin crystals and has a white streak. Crystals are nonfluorescent under short-wavelength ultraviolet light and the beam of the electron microprobe. The (Mohs') hardness is approximately 6. Density has been calculated as 3.54 g/cm³ but could not be measured directly because of contamination by glass and crystals that are attached to many of the individual grains.

Optically, esseneite is biaxial negative with $2V_X = 77°$ (±5°). The indices of refraction are $\alpha = 1.795$, $\beta = 1.815$, and $\gamma = 1.825$ (all ±0.005). Pleochroism is quite distinctive with the following formula: $X$ = lemon yellow; $Y$ = greenish yellow; and $Z$ = apple-green. Dispersion of the optic axes is strong, $r < v$, and the $X$ and $Z$ vibration directions show strong inclined dispersion. Orientation of the indicatrix has $Y = \mathbf{b}$ and $Z \wedge \mathbf{c} = 9°$ (±3°) in the acute angle $\beta$. Although esseneite and aegirine have a similar appearance in thin section, they may be distinguished by their pleochroism and by the angle $Z \wedge \mathbf{c}$ in esseneite vs. the angle $X \wedge \mathbf{c}$ in aegirine.

## Mineral chemistry and X-ray crystallography

Samples of esseneite (DR-8) were chemically analyzed using a fully automated CAMECA Camebax microprobe at the University of Michigan. Wavelength-dispersive analyses were conducted on separated grains and on crystals within polished thin sections using an accelerating voltage of 15 kV and a sample current of 10 nA. The standards used were diopside (Ca, Mg, Si), jadeite (Al, Na), synthetic ferrosilite (Fe), geikielite (Ti), and rhodonite (Mn). Following refinement of the crystal structure, an additional analysis was conducted on the single crystal used for the structure refinement by separating the crystal from the spindle and preserving it in a resin-cast grain mount. The crystal habit was utilized by exposing and analyzing a cleavage surface, thus minimizing polishing of the sample. Results of the actual single-crystal analysis together with the average composition of 43 separated mineral grains and thin-section analyses are presented in Table 1. The apparent differences between the analyses with respect to Al and $Fe^{3+}$ are inferred to be due to possible microchemical and/or structural domains within the single crystal and are described more fully in the results.

An X-ray powder-diffraction pattern was obtained using a powder diffractometer with CuK$\alpha$ radiation and Si as an internal standard with a graphite monochromator (Table 2). The unit-cell parameters, refined by least-squares using the powder-diffraction data, are $a = 9.79(1)$, $b = 8.822(9)$, $c = 5.37(1)$ Å, and $\beta = 105.81(9)°$. These data are in excellent agreement with the cell parameters of synthetic $CaFeAlSiO_6$ (Hijikata, 1968; Akasaka and Onuma, 1980; Ghose et al., 1975). A small cleavage fragment of esseneite was studied by the Weissenberg method, and the results are consistent with space group $C2/c$ as originally determined by Ghose et al. (1975) for synthetic FATs. Other space groups such as $C2$, $P2/n$, $C1$, and $P2_1/n$ are possible owing to Al-Si ordering. If present, there must be antiphase domains, unobservable by single-crystal X-ray diffraction, such that the Al-Si distribution averaged over the crystal is consistent with space group $C2/c$. This possibility is currently being evaluated by high-resolution TEM studies.

## Structure refinement

A crystal fragment approximately 0.06 × 0.07 × 0.32 mm in size from sample DR-8 was selected for X-ray structure analysis. A chemical analysis from a surface of this crystal is presented in Table 1. The crystal was mounted parallel to the **c** axis, and intensities of 509 reflections were measured using an automated Supper-Pace X-ray diffractometer with Weissenberg equi-inclination geometry, monochromatized Mo$K\alpha$ radiation, and a scanning rate of 2° 2$\theta$/min. The data were converted to

Table 2. X-ray powder-diffraction data

| $I/I_0$ | $d_{obs}$ | $d_{calc}$ | $hkl$ |
|---|---|---|---|
| 10 | 6.45 | 6.44 | 110 |
| 5 | 4.71 | 4.71 | 200 |
| 2 | 4.43 | 4.46 | $11\bar{1}$ |
| | | 4.41 | 020 |
| 2 | 3.72 | 3.71 | 111 |
| 20 | 3.214 | 3.220 | 220 |
| 100 | 3.000 | 2.994 | $22\bar{1}$ |
| 60 | 2.960 | 2.957 | 310 |
| 20 | 2.909 | 2.909 | $31\bar{1}$ |
| 30 | 2.576 | 2.570 | $11\bar{2}$ |
| | | 2.582 | $20\bar{2}$ |
| 40 | 2.554 | 2.555 | $13\bar{1}$ |
| 70 | 2.526 | 2.529 | 221 |
| 10 | 2.322 | 2.323 | 311 |
| 10 | 2.252 | 2.257 | 112 |
| | | 2.254 | $31\bar{2}$ |
| 5 | 2.147 | 2.146 | 330 |
| 20 | 2.125 | 2.127 | $33\bar{1}$ |
| 15 | 2.110 | 2.111 | $42\bar{1}$ |
| 20 | 2.031 | 2.039 | $40\bar{2}$ |
| | | 2.029 | 041 |
| 10 | 1.980 | 1.983 | $13\bar{2}$ |
| 20 | 1.734 | | |
| 5 | 1.686 | | |
| 2 | 1.677 | | |
| 5 | 1.650 | | |
| 10 | 1.627 | | |
| 7 | 1.612 | | |
| 30 | 1.545 | | |
| 25 | 1.430 | | |
| 20 | 1.409 | | |
| 10 | 1.370 | | |

structure-factor amplitudes by correction for the Lorentz factor, polarization, and absorption ($\mu_1 = 38.52$ cm$^{-1}$). A total of 47 reflections had intensities below the minimum observable limit of detection.

The structure refinement was carried out using the least-squares refinement program RFINE II (Finger, 1972) using neutral-atom scattering factors. Beginning with the structure parameters of fassaite (Peacor, 1967) and using isotropic temperature factors, the refinement rapidly converged to an $R$ factor of 11.2%. Form factors were held constant with occupancies $Mg_{0.30}Fe_{0.70}$, $Ca_{1.0}Na_{0.0}$, and $Si_{0.55}Al_{0.45}$ for the M1, M2, and T sites, respectively. Using anomalous scattering factors and anisotropic temperature factors and varying the occupancies, the refinement converged to an unweighted $R$ factor of 5.3% for all reflections. At this point, the occupancy values for the M2 site were considered unrealistic when compared to the analytical data and the occupancy values for the M1 and T sites. The variance-covariance matrix and general character of the refinement indicated that there was a strong correlation between the anisotropic temperature factors and occupancies of M1, M2, and T, such that all parameters could not be independently varied. Therefore the refinement was continued with the M2 site constrained to 97% Ca and 3% Na as indicated by the chemical analysis. Several cycles with the M2 and T occupancies varying and with different form factors gave values consistent with this occupancy. Final cycles proceeded to yield unweighted $R$ factors of 5.5% for all reflections and 4.6% excluding unobserved reflections. The final values for the refined atomic parameters of esseneite are given in Table 3. Interatomic distances and angles were computed using the variance-covariance matrix of the structure refinement. Values of selected cation–oxygen bond distances

Table 4. Values of selected cation–oxygen bond distances (Å) of esseneite

| Tetrahedron | | M1 octahedron | | M2 polyhedron | |
|---|---|---|---|---|---|
| T–O(1) | 1.646(3) | M1–2O(2) | 1.971(3) | M2–2O(1) | 2.393(4) |
| –O(2) | 1.646(3) | –2O(1) | 2.055(5) | –2O(2) | 2.406(5) |
| –O(3) | 1.698(4) | –2O(1)′ | 2.125(3) | –2O(3) | 2.536(4) |
| –O(4) | 1.714(4) | | | –2O(3)′ | 2.644(4) |
| Avg. | 1.682 | | | | |

Table 3. Refined atomic parameters of esseneite (standard deviations in parentheses)

| Atom | $X$ | $Y$ | $Z$ | Occupancy | $\beta_{11}$ | $\beta_{22}$ | $\beta_{33}$ | $\beta_{12}$ | $\beta_{13}$ | $\beta_{23}$ | $B_{eq}$ |
|---|---|---|---|---|---|---|---|---|---|---|---|
| M1 | 0 | 0.0942(1) | ¾ | | 0.00121(8) | 0.00101(4) | 0.00575(7) | 0 | 0.00054(4) | 0 | 0.54 |
| Fe | | | | 0.58(3) | | | | | | | |
| Al | | | | 0.42(3) | | | | | | | |
| M2 | 0 | 0.6918(1) | ¾ | | 0.00304(17) | 0.00238(1) | 0.00942(8) | 0 | 0.00122(7) | 0 | 1.20 |
| Ca | | | | 0.97 | | | | | | | |
| Fe | | | | 0.03 | | | | | | | |
| T | 0.2117(1) | 0.4057(1) | 0.7764(2) | | 0.00070(2) | 0.00059(1) | 0.00458(25) | −0.00017(2) | 0.00057(5) | −0.00040(4) | 0.42 |
| Si | | | | 0.54(3) | | | | | | | |
| Al | | | | 0.46(3) | | | | | | | |
| O1 | 0.3888(3) | 0.4123(3) | 0.8659(6) | | 0.00295(25) | 0.00310(2) | 0.00901(70) | −0.00008(7) | 0.00167(33) | 0.00040(29) | 1.23 |
| O | | | | 1 | | | | | | | |
| O2 | 0.1366(3) | 0.2411(4) | 0.6799(6) | | 0.00392(1) | 0.00410(11) | 0.00973(10) | −0.00027(7) | 0.00206(20) | 0.00020(11) | 1.53 |
| O | | | | 1 | | | | | | | |
| O3 | 0.1468(3) | 0.4802(4) | 0.0124(6) | | 0.00300(8) | 0.00330(30) | 0.01474(34) | 0.00011(11) | 0.00188(7) | −0.00060(20) | 1.54 |
| O | | | | 1 | | | | | | | |

Table 5. Magnitudes and orientations of thermal ellipsoids of vibration of esseneite

| Atom | Axis | rms displacement (Å) | Angle (°) with respect to a | b | c |
|---|---|---|---|---|---|
| M1 | 1 | 0.076(3) | 90 | 0 | 90 |
| | 2 | 0.081(3) | 162(8) | 90 | 108(8) |
| | 3 | 0.097(3) | 108(8) | 90 | 18(8) |
| M2 | 1 | 0.092(3) | 90 | 0 | 90 |
| | 2 | 0.111(2) | 121(23) | 90 | 149(23) |
| | 3 | 0.116(2) | 31(23) | 90 | 121(23) |
| T | 1 | 0.057(4) | 56(17) | 37(16) | 78(5) |
| | 2 | 0.068(3) | 146(17) | 56(16) | 86(8) |
| | 3 | 0.085(3) | 93(7) | 102(5) | 13(5) |
| O1 | 1 | 0.106(6) | 103(10) | 113(14) | 27(14) |
| | 2 | 0.123(5) | 106(26) | 148(20) | 116(14) |
| | 3 | 0.132(6) | 22(20) | 111(24) | 84(15) |
| O2 | 1 | 0.120(5) | 109(15) | 113(15) | 31(8) |
| | 2 | 0.133(5) | 131(35) | 125(38) | 121(18) |
| | 3 | 0.139(5) | 46(35) | 136(32) | 94(21) |
| O3 | 1 | 0.120(6) | 17(11) | 100(20) | 77(13) |
| | 2 | 0.130(6) | 94(21) | 157(18) | 112(18) |
| | 3 | 0.143(5) | 106(11) | 110(17) | 26(16) |

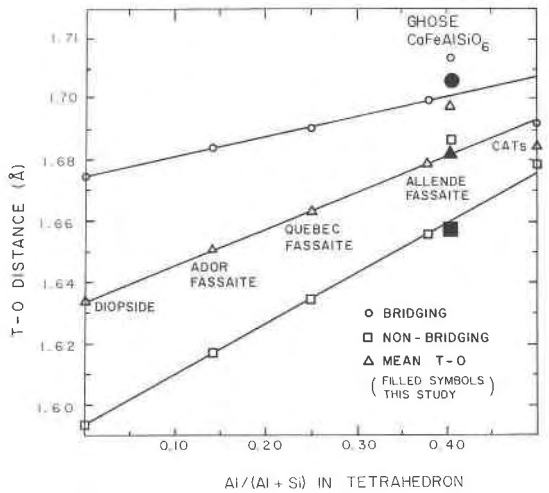


Fig. 2. Plot of average tetrahedral cation–oxygen bond distances as a function of Al/(Al + Si) in the tetrahedral site for aluminous pyroxenes (after Hazen and Finger, 1977).

are presented in Table 4, and the magnitudes and orientations of the thermal-vibration ellipsoids are presented in Table 5.

## Results

### Cation order

The detailed topology of Al and $Fe^{3+}$-rich Ca-clinopyroxenes has been described in detail by Ghose et al. (1986). Because the topology of the esseneite structure is consistent with those relations, they are not reviewed here. Rather, here we are primarily concerned with the degree of Al and $Fe^{3+}$ substitution in the tetrahedrally coordinated sites and its relation to site occupancy of the M1 site. Because the chemical analyses, M2 polyhedron topology, and refined occupancies were all consistent with Ca and only minor Na in M2, only those cations were inferred to occupy the M2 site.

Figure 2 is a plot of T–O distances versus tetrahedral Al/(Al + Si) occupancy for aluminous pyroxenes. The well-defined linearity confirms that they are accurately determined. Using Figure 2 and the refined average T–O distance of 1.682 Å (Table 4), the T site is predicted to have 41% Al. This agrees well with the value determined from the average chemical analysis (Table 1), which was derived by stoichiometry such that cations in the tetrahedral site were assigned in order of preference Si > Al > $Fe^{3+}$. Ghose et al. (1986) have suggested that large cations in the M1 site cause an increase in T–O distances for bridging oxygens. Slightly larger T-O distances than those predicted for esseneite (Fig. 2) may therefore be a result of the dominance of Fe in the M1 site as compared to the other pyroxenes that have Al in the M1 site. By contrast, Ghose et al. (1986) determined the average T–O distance (1.698 Å) for a synthetic FATs pyroxene for which the tetrahedral occupancy is $Si_{0.50}Al_{0.41}Fe^{3+}_{0.09}$. This value plots far from the linear trend of Figure 2, reflecting the large radius of $Fe^{3+}$ relative to Si or Al. Fractions of $Fe^{3+}$ much less than those observed by Ghose et al. (1986) cause T–O distances to be inordinately large. In addition, refinement of the occupancy of the T site with Al and Si form factors gives rise to an occupancy of 0.46 Al, very near to the value predicted from analytical data and deduced from T–O distances, especially in light of the near equality in Al and Si form factors. Even very minor amounts of $Fe^{3+}$ would result in a major apparent increase in the amount of Si relative to Al. As a further check for possible tetrahedral $Fe^{3+}$, refinements were conducted with Fe and Si form factors for the T site. In addition, refinements were run with fixed amounts of all elements except $Fe^{3+}$ and Al as indicated by the average chemical analysis (Table 1) and allowing only $Fe^{3+}$ and Al to vary on the M1 and T sites. Results of these refinements indicate that, within error of the refinement, there is no tetrahedral $Fe^{3+}$. We therefore conclude that there is no detectable $Fe^{3+}$ occupying the tetrahedral site and that 0.46 Al substitutes for Si.

The occupancy of the M1 octahedral site was refined with Fe and Mg form factors since the chemical analysis, combined with the conclusions regarding the M2 and T sites as discussed above, indicated that these cations are dominant in that site. Al is also present, but in light of the similarity in Mg and Al form factors, any Al present can be approximated as Mg in that site. The final refined occupancies are 0.58 $Fe^{3+}$ and 0.42 Mg, in good agreement with the chemical analyses. Additional refinements using Fe and Al form factors with Mg constrained by the average chemical analysis (Table 1) gave values consistent with these M1 occupancies.

The overall structure refinement is in fair agreement with the average chemical analysis presented in Table 1.

Because the chemical analysis from a portion (cleavage face) of the refined single crystal (Table 1) varies somewhat from the composition implied by the structure refinement and from the average chemical analysis (especially with respect to Fe and Al), we conclude that the chemical analysis obtained on the cleavage face is not entirely representative of that crystal. It is possible that microchemical variations (zoning) gave rise to an aberrant chemical analysis. Considering the agreement between the structure refinement and the *average* chemical analysis, the cleavage-face chemical analysis is suspect.

### Implications

The preference of Al and $Fe^{3+}$ for the M1 and T sites in synthetic FATs has been evaluated by several workers (Ohashi and Hariya, 1970; Huckenholz et al., 1974; Ghose et al., 1975, 1986; Kurepin et al., 1981) indicating that a small amount of $Fe^{3+}$ substitutes in the tetrahedral site. Because esseneite and synthetic FATs were formed at equivalent temperatures and because synthetic FATs contains tetrahedral $Fe^{3+}$ but esseneite does not, there is a strong suggestion of a cooling-rate dependence for the partitioning of Al and $Fe^{3+}$ into the tetrahedral and M1 octahedral sites.

The conditions under which esseneite formed are considered to be rapid by geologic standards. Indeed, a variety of features that are produced by quenching, such as spinifex-like olivines, skeletal and hopper phenocrysts, and a glass phase, are observed in thin sections of paralava (Cosca and Essene, 1985). Similar textures have been produced experimentally by quenching basalt with cooling rates of 30–120°C/h (Lofgren et al., 1974). Although cooling histories of paralava are poorly understood, the distribution of $Fe^{3+}$ and Al in esseneite from paralava, when compared to that in the synthetic FATs, suggests that rapid geologic quenches (paralava) are still relatively slow when compared to laboratory quenches. Kurepin et al. (1981) annealed synthetic FATs at several temperatures and determined an approximate linear temperature dependence of ordering of Al and $Fe^{3+}$ between the M1 and T sites using Mössbauer analysis. Their samples were quenched over time intervals of only a few seconds, and the results imply an equilibrium relation. Nevertheless, $Fe^{3+}$ substitution may not occur in the T sites of natural pyroxenes, as some workers have suggested (Akasaka, 1983; Kurepin et al., 1981), given that it is absent in natural samples that have been quenched over a very short time interval in geologic terms.

## Discussion

Laboratory experiments carried out in air have shown that esseneite ($CaFeAlSiO_6$) exhibits complete solid solution with diopside ($CaMgSi_2O_6$) (Hijikata, 1968; Hijikata and Onuma, 1969). At high pressure, Ohashi and Hariya (1975a) demonstrated that esseneite breaks down to unspecified solid solutions of garnet, spinel, and pyroxene. Additional experiments by Hijikata (1973) showed that with increasing pressure, diopside has increased solid solution favoring the CaTs ($CaAlAlSiO_6$) component. However, the degree of fassaite solid solution in diopside has been a topic of controversy. Ginzburg (1969) proposed a miscibility gap between diopside and fassaite based upon coexisting fassaite and diopside from a metasomatized dolerite at Vilyuy, Yakutia. In contrast, Shedlock and Essene (1979) examined numerous diopside-fassaite solid solutions from a tactite in Montana with compositions plotting well within the proposed solvus of Ginzburg, implying an absence of such a solvus. They argued that the break in slope of pyroxene cell dimensions along the binary join $CaMgSi_2O_6$-$CaAlAlSiO_6$ (Sakata, 1957) was probably caused by a depletion in the $CaAlAlSiO_6$ component in melilite and anorthite and was not evidence for a solvus. Subsequent experimental work by Onuma et al. (1981) has revealed no solvus in the system CaTs-FATs-Di at subsolidus temperatures. Therefore, the combination of laboratory studies and observations of natural occurrences of fassaite of widely varying chemistry suggests that there is complete solid solution among pyroxenes in the system $CaMgSi_2O_6$-$CaFeAlSiO_6$-$CaAlAlSiO_6$.

The occurrence of esseneite in paralava indicates that this pyroxene is stable at high temperatures, with locally high oxygen fugacities evidenced by the high $Fe^{3+}/Fe^{2+}$ ratios. Indeed, Oba and Onuma (1978), Onuma et al. (1981), and Onuma (1983) have suggested that esseneite is stable along the binary join $CaMgSi_2O_6$-$CaFeAlSiO_6$ at high temperature and at $f_{O_2}$ values approaching the hematite-magnetite buffer. Onuma et al. (1981) concluded that the amount of the FATs component in fassaitic pyroxenes is principally a function of $f_{O_2}$, whereas the CaTs component is pressure dependent. Esseneite is also stable at pressures up to 45 kbar in the presence of hematite (Ohashi and Hariya, 1975b), although high $f_{O_2}$ at this pressure seems unlikely in the mantle. Nevertheless, high temperature and high oxygen fugacity are critical to the stabilization of esseneite, and except for the unusual environment giving rise to paralava, such conditions are unlikely to occur, perhaps explaining why esseneite-rich pyroxenes have not been previously reported.

The thermodynamic properties of esseneite have been estimated in order to calculate phase equilibria for assemblages occurring in paralava. The $S^{\circ}_{298}$ was estimated from the measured entropies of CaTs (Robinson et al., 1982) plus acmite (Bennington and Brown, 1982) minus jadeite (Robie et al., 1978). The thermal expansivity and compressibility were assumed equivalent to CaTs (Haselton et al., 1984; Robinson et al., 1982). The molar volume was calculated from this paper. The free energy of esseneite was estimated from the experimental reversal of Huckenholz et al. (1974) for the reaction

$$\underset{\text{grandite}}{Ca_3(Fe^{3+}Al)Si_3O_{12}} = \underset{\text{Woll}}{2CaSiO_3} + \underset{\text{Ess}}{CaFe^{3+}AlSiO_6}. \quad (1)$$

Because the free energy of grandite ($grossular_{50}andradite_{50}$) is unknown, it was calculated from available experiments

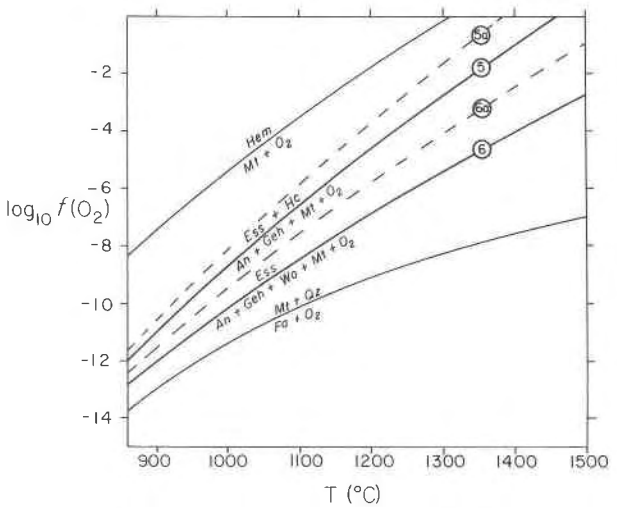


Fig. 3. Graph of temperature vs. oxygen fugacity for equilibria in paralava (see text) relative to the hematite-magnetite and quartz-fayalite-magnetite buffers. Dashed lines show shifts in the positions of the curves for reduced activities of spinels.

(Huckenholz et al., 1974, 1981) on garnet solid solutions. Grandite free energy was calculated from the free energies of grossular (Robinson et al., 1982) and andradite by the relation

$$Ca_3Fe^{3+}AlSi_3O_{12} = 0.5Ca_3Fe_2^{3+}Si_3O_{12} + 0.5Ca_3Al_2Si_3O_{12}, \quad (2)$$

taking into account nonideal mixing of $Fe^{3+}$ and Al (Cosca et al., 1986). The free energy of andradite was first estimated from the experimental reversals of Huckenholz and Yoder (1971) for the reaction

$$\underset{\text{And}}{Ca_3Fe_2^{3+}Si_3O_{12}} = \underset{\text{Hem}}{Fe_2O_3} + \underset{\text{Woll}}{3CaSiO_3}. \quad (3)$$

The molar volume for andradite was taken from Robie et al. (1978) and the thermal expansivity and compressibility were taken from Skinner (1966) and Birch (1966). Substitution of grandite free energy into Equation 1 allows calculation of esseneite free energy at experimental conditions. Grandite entropy was estimated from the entropies of andradite (Robie, pers. comm., 1986) and grossular (Robinson et al., 1982) with a one-site mixing term. Data for grandite thermal expansivity (Skinner, 1966), compressibility (Babuska et al., 1978), and entropy allow calculation of esseneite free energy at 298 K ($\Delta G^0_{298}$). The calculated thermodynamic values for esseneite are as follows: $\Delta G^0_{298} = -2705.8$ kJ; $\Delta H^0_{298} = -2871.1$ kJ; and $S^0_{298} = 177.0\ J \cdot mol^{-1} \cdot K^{-1}$.

Use of the above thermodynamic data now make it possible to evaluate the stability of esseneite-bearing reactions through phase-equilibrium calculations. The assemblage anorthite, esseneite, melilite solid-solution, and magnetite-hercynite solid solution occurring in paralava allow certain equilibria to be applied. For example:

$$\underset{\text{An}}{4CaAl_2Si_2O_8} + \underset{\text{Mt}}{2Fe_3O_4} = \underset{\text{Ess}}{4CaFe^{3+}AlSiO_6} + \underset{\text{Hc}}{2FeAl_2O_4} + \underset{\text{Qz}}{4SiO_2}. \quad (4)$$

Reaction 4 is a solid-solid reaction, suggesting that anorthite and magnetite react to form esseneite component in pyroxene, along with hercynite and quartz. The position of this reaction calculated in $P$-$T$ space suggests that anorthite and magnetite are stable at reasonable geologic conditions. However, at high temperatures and with reduced activities of the esseneite component in pyroxene, the right-hand side of the reaction may be stabilized. Mineral assemblages corresponding to Reaction 4 have been identified in paralava, and the esseneite substitution is greatly reduced in the pyroxenes from these samples, which is consistent with the calculated equilibria.

Paralava assemblages that consistently contain the highest degree of the esseneite component in clinopyroxene may be expressed by the following reaction:

$$\underset{\text{An}}{6CaAl_2Si_2O_8} + \underset{\text{Geh}}{6Ca_2Al_2SiO_7} + \underset{\text{Mt}}{7Fe_3O_4} + O_2 = \underset{\text{Ess}}{18CaFe^{3+}AlSiO_6} + \underset{\text{Hc}}{3FeAl_2O_4}. \quad (5)$$

A less common assemblage, but also containing high proportions of the esseneite component may be related by the reaction

$$\underset{\text{An}}{3CaAl_2Si_2O_8} + \underset{\text{Geh}}{3Ca_2Al_2SiO_7} + \underset{\text{Woll}}{3CaSiO_3} + \underset{\text{Mt}}{4Fe_3O_4} + O_2 = \underset{\text{Ess}}{12CaFe^{3+}AlSiO_6}. \quad (6)$$

Reactions 5 and 6 are oxidation-reduction reactions and have been calculated in $T$-$f_{O_2}$ space (Fig. 3). The positions of reactions 5 and 6 lie between the quartz-fayalite-magnetite and hematite-magnetite buffers (Fig. 3). Adjustment of these endmember reactions for reduced activities of the spinel phase (Petric et al., 1981) (e.g., $X_{Mt} = X_{Hc} = 0.5$, Reactions 5a and 6a, Fig. 3) shifts their location to temperatures and oxygen fugacities closer to the hematite-magnetite buffer. Since nearest endmember esseneite is found in silica-undersaturated rocks containing melilite, anorthite, and magnetite-hercynite solid solutions, it is quite likely that Reaction 5 is driven to the right under the conditions of formation of esseneite in paralava. Although the exact positions of the esseneite equilibria must be corrected for the specific activities of the appropriate components in a given assemblage, it is evident that esseneite-rich pyroxenes are generally favored by high temperature and high oxygen fugacity.

*Note added in proof*: Hooper and Foit (1986) and Foit et al. (1987) recently have reported a large number of analyses for pyroxenes from a coal-fire buchite near Buffalo, Wyoming. Many of their analyses have >50% $CaFeSiAlO_6$ and are presumably esseneites. Some of their

pyroxene analyses have inadequate Al to fill the tetrahedral site and require up to 32% $Fe^{3+}$ in that site.

## Acknowledgments

We are grateful to Subrata Ghose for sharing data on synthetic FATs prior to publication. We also wish to thank F. F. Foit and R. L. Hooper who shared unpublished data for a similar pyroxene found in a similar locality. Special gratitude is owed to W. C. Bigelow and C. H. Henderson for maintaining the microbeam facilities at the University of Michigan. The electron-microprobe analyzer used in this work was acquired under Grant EAR-82-12764 from the National Science Foundation. We thank Eric Essene for his uncompromising acceptance of the mineral name and for reviewing early drafts of the manuscript. We are grateful to J. R. Smyth and T. C. McCormick for their comments on the manuscript. This project was funded in part by grants from Sigma Xi and the Turner Fund (University of Michigan) to M.A.C.

## References

Akasaka, M. (1983) $^{57}$Fe Mössbauer study of clinopyroxenes in the join $CaFeAlSiO_6$-$CaTiAl_2O_6$. Physics and Chemistry of Minerals, 9, 205–211.

Akasaka, M., and Onuma, K. (1980) The join $CaMgSi_2O_6$-$CaFeAlSiO_6$-$CaTiAlSiO_6$ and its bearing on the Ti-rich fassaitic pyroxenes. Contributions to Mineralogy and Petrology, 71, 301–312.

Babuska, V., Fiala, J., Kumazawa, M., Ohno, I., and Sumino, Y. (1978) Elastic properties of garnet solid-solution series. Physics of the Earth and Planetary Interiors, 16, 157–176.

Bennington, K.O., and Brown, R.R. (1982) Thermodynamic properties of synthetic acmite ($NaFe^{3+}Si_2O_6$). U.S. Bureau of Mines Report of Investigations, 8621, 1–18.

Bentor, Y.K. (1984) Combustion-metamorphic glasses. Journal of Non-Crystalline Solids, 67, 433–448.

Bentor, Y.K., Kastner, M., Perlman, I., and Yellin, Y. (1981) Combustion metamorphism of bituminous sediments and the formation of melts of granitic and sedimentary composition. Geochimica et Cosmochimica Acta, 45, 2229–2255.

Birch, Francis. (1966) Compressibility; elastic constants. Geological Society of America Memoir 97, 97–173.

Cosca, M.A., and Essene, E.J. (1985) Paralava chemistry and conditions of formation, Powder River Basin, Wyoming (abstr.) EOS, 66, 396.

Cosca, M.A., Moecher, D.M., and Essene, E.J. (1986) Activity-composition relations for the join grossular-andradite and application to calc-silicate assemblages: Geological Society of America Abstracts with Programs, 18, 572.

Davis, A.M. (1984) A scandalously refractory inclusion in Ornans. Meteoritics, 19, 214.

Deer, W.A., Howie, R.A., and Zussman, J. (1978) Rock-forming minerals, 2nd ed., vol. 2A, p. 399–414. Wiley, New York.

Devine, J.D., and Sigurdsson, H. (1980) Garnet-fassaite calc-silicate nodule from La Soufrière, St. Vincent. American Mineralogist, 65, 302–305.

Dobretsov, N.L. (1968) Paragenetic types and compositions of metamorphic pyroxenes. Journal of Petrology, 9, 358–357.

Dodd, R.T. (1971) Calc-aluminous insets in olivine of the Sharps chondrite. Mineralogical Magazine, 38, 451–458.

Dowty, E., and Clark, J.R. (1973) Crystal structure refinement and optical properties of a $Ti^{3+}$ fassaite from the Allende meteorite. American Mineralogist, 58, 230–242.

Essene, E.J., and Peacor, D.R. (1987) Petedunnite ($CaZnSi_2O_6$), a new zinc clinopyroxene from Franklin, New Jersey, and phase equilibria for zincian pyroxenes. American Mineralogist, 72, 157–166.

Finger, L.W. (1972) RFINE II: A Fortran IV computer program for structure factor calculation and least-square refinement of crystal structures. Geophysical Laboratory, Washington, D.C.

Foit, F.F., Jr., Hooper, R.L., and Rosenberg, P.E. (1987) An unusual pyroxene, melilite, and iron oxide mineral assemblage in a coal-fire buchite from Buffalo, Wyoming. American Mineralogist, 72, 137–147.

Ghose, S., Wan, C., Okamura, F.P., Ohashi, H., and Weidner, J.R. (1975) Site preference and crystal chemistry of transition metal ions in pyroxenes and olivines. Acta Crystallographica, sect. A, 31, 76.

Ghose, S., Okamura, F.P., and Ohashi, H. (1986) The crystal structure of $CaFe^{3+}SiAlO_6$ and the crystal chemistry of $Fe^{3+}$-$Al^{3+}$ substitution in calcium Tschermak's pyroxene. Contributions to Mineralogy and Petrology, 92, 530–535.

Ginzburg, I.V. (1969) Immiscibility of the natural pyroxenes diopside and fassaite and the criterion for it. Akademii Nauk USSR Doklady, 186, 423–426.

Gross, S. (1977) The mineralogy of the Hatrurium Formation, Israel. Geological Survey of Israel Bulletin, 70, 1–80.

Hall, R. (1980) Contact metamorphism by an ophiolite peridotite from Neyriz, Iran. Science, 208, 1259–1262.

Haselton, H.T., Jr., Hemingway, B.S., and Robie, R.A. (1984) Low-temperature heat capacities of $CaAl_2SiO_6$ glass and pyroxene and thermal expansion of $CaAl_2SiO_6$ pyroxene. American Mineralogist, 69, 481–489.

Hazen, R.M., and Finger, L.W. (1977) Crystal structure and compositional variation of Angra Dos Reis fassaite. Earth and Planetary Science Letters, 35, 357–362.

Hijikata, K. (1968) Unit-cell dimensions of the clinopyroxenes along the join $CaMgSi_2O_6$-$CaFe^{3+}AlSiO_6$. Journal of the Faculty of Science, Hokkaido University, ser. IV, 14, 149–157.

——— (1973) Phase relations in the system $CaMgSi_2O_6$-$CaAl_2SiO_6$ at high pressures and temperatures. Journal of the Faculty of Science, Hokkaido University, ser. IV, 16, 167–177.

Hijikata, K., and Onuma, K. (1969) Phase equilibria of the system $CaMgSi_2O_6$-$CaFe^{3+}AlSiO_6$ in air. Japanese Association of Mineralogists, Petrologists and Economic Geologists Journal, 62, 209–217.

Hooper, R.L., and Foit, F.F., Jr. (1986) Pyroxenes and melilites with extensive tetrahedral $Fe^{3+}$ substitution from a coal fire buchite near Buffalo, Wyoming (abs.). EOS, 67, 1270.

Huckenholz, H.G., and Yoder, H.S. Jr. (1971) Andradite stability relations in the $CaSiO_3$-$Fe_2O_3$ join up to 30 kbar. Neues Jahrbuch für Mineralogie Abhandlungen, 114, 246–280.

Huckenholz, H.G., Lindhuber, W., and Springer, J. (1974) The join $CaSiO_3$-$Al_2O_3$-$Fe_2O_3$ of the $CaO$-$Al_2O_3$-$Fe_2O_3$-$SiO_2$ quaternary system and its bearing on the formation of granditic garnets and fassaitic pyroxenes. Neues Jahrbuch für Mineralogie Abhandlungen, 121, 160–207.

Huckenholz, H.G., Lindhuber, W., and Fehr, K.T. (1981) Stability relationships of grossular + quartz + wollastonite + anorthite. Neues Jahrbuch für Mineralogie Abhandlungen, 142, 223–247.

Kornprobst, J., Piboule, M., Boudeulle, M., and Roux, L. (1982) Corundum-bearing garnet pyroxenites at Beni-Bousera (Morocco): An exceptionally Al-rich clinopyroxene from "grospydites" associated with ultramafic rocks. Terra Cognita, 2, 257–259.

Kurepin, V.A., Polshin, E.V., and Alibekov, G.I. (1981) Intracrystalline distribution of the cations $Fe^{3+}$ and Al in the clinopyroxene $CaFe^{3+}AlSiO_6$. Mineralogisheskii Zhurhal, 3, 83–88.

Lal, R.K., Ackermand, D., Raith, M., Raase, P., and Seifert, F. (1984) Sapphirine-bearing assemblages from Kiranur, southern India: A study of chemographic relationships in the $Na_2O$-$FeO$-$MgO$-$Al_2O_3$-$SiO_2$-$H_2O$ system. Neues Jahrbuch für Mineralogie Abhandlungen, 150, 121–152.

LeBas, M. (1962) The role of aluminum in igneous clinopyroxenes with relation to their parentage. American Journal of Science, 260, 267–288.

Lofgren, G., Donaldson, C.H., Williams, R.J., Mullins, O., Jr., and Usselman, T.M. (1974) Experimentally reproduced textures and mineral chemistry of Apollo 15 quartz normative

basalts. 5th Lunar and Planetary Science Conference Proceedings, 1, 549–569.

Oba, T., and Onuma, K. (1978) Preliminary report of the join $CaMgSi_2O_6$-$CaFe^{3+}AlSiO_6$ at low oxygen fugacity. Journal of the Faculty of Science, Hokkaido University, ser. IV, 18, 433–444.

Ohashi, H., and Hariya, Y. (1970) Order-disorder of ferric iron and aluminum in Ca-rich clinopyroxene. Proceedings of the Japanese Academy, 46, 684–687.

——— (1975a) Decomposition of $CaFe^{3+}AlSiO_6$ pyroxene at high pressure and low oxygen partial pressure. Japanese Association of Mineralogists, Petrologists, and Economic Geologists Journal, 70, 347–351.

——— (1975b) Phase relations of $CaFeAlSiO_6$ pyroxene at high pressures and temperatures. Japanese Association of Mineralogists, Petrologists, and Economic Geologists Journal, 70, 93–95.

Onuma, K. (1983) Effect of oxygen fugacity on fassaitic pyroxene. Journal of the Faculty of Science, Hokkaido University, ser. IV, 20, 185–194.

Onuma, K., Akasaka, M., and Yagi, K. (1981) The bearing of the system $CaMgSi_2O_6$-$CaAl_2SiO_6$-$CaFeAlSiO_6$ on fassaitic pyroxene. Lithos, 14, 173–182.

Peacor, D.R. (1967) Refinement of the crystal structure of a pyroxene of formula $M_IM_{II}(Si_{1.5}Al_{0.5})O_6$. American Mineralogist, 52, 31–41.

Petric, A., Jacob, K.T., and Alcock, C.B. (1981) Thermodynamic properties of $Fe_3O_4$-$FeAl_2O_4$ spinel solid solutions. American Ceramic Society Journal, 64, 632–639.

Prinz, M., Keil, K., Hlava, P.F., Berkley, J.L., Gomes, C.B., and Curvello, W.S. (1977) Studies of Brazilian meteorites, III. Origin and history of the Angra Dos Reis achondrite. Earth and Planetary Science Letters, 35, 317–330.

Robie, R.A., Hemingway, B.S., and Fisher, J.R. (1978) Thermodynamic properties of minerals and related substances at 298.15 K and 1 bar ($10^5$ pascals) and at higher temperatures. U.S. Geological Survey Bulletin 1452.

Robinson, G.R., Jr., Haas, J.L., Jr., Schafer, C.M., and Haselton, H.T. (1982) Thermodynamic and thermophysical properties of selected phases in the $MgO$-$SiO_2$-$H_2O$-$CO_2$, $CaO$-$Al_2O_3$-$SiO_2$-$H_2O$-$CO_2$, and $Fe$-$FeO$-$Fe_2O_3$-$SiO_2$ chemical systems, with special emphasis on the properties of basalts and their mineral components. U.S. Geological Survey Open-File Report 83–79.

Sakata, Y. (1957) Unit cell dimensions of synthetic aluminum diopsides. Japanese Journal of Geology and Geography, 28, 161–168.

Shatskiy, V.S., Sobolev, N.V., and Pavlyuchenko, V.S. (1985) Fassaite-garnet-anorthite xenolith from the Udachnaya kimberlite pipe, Yakutia. Akademii Nauk SSSR Doklady, 272, 1, 188–192.

Shedlock, R.J., and Essene, E.J. (1979) Mineralogy and petrology of a tactite near Helena, Montana. Journal of Petrology, 20, 71–97.

Skinner, B.J. (1966) Thermal expansion. Geological Society of America Memoir 97, 75–96.

Treiman, A.H. (1982) The Oka carbonatite complex, Quebec: Aspects of carbonatite petrogenesis. Ph.D. thesis, University of Michigan, Ann Arbor.

Williams-Jones, A.E. (1981) Thermal metamorphism of siliceous limestone in the aureole of Mount Royal, Quebec. American Journal of Science, 281, 673–696.

Manuscript received January 2, 1986
Manuscript accepted October 22, 1986